RESEARCH ARTICLE

Sector Unit-Cell Methodology for the Design of Sub-6 GHz 5G MIMO Antennas

JAIME MOLINS-BENLLIURE, (Student Member, IEEE),
MARTA CABEDO-FABRÉS, (Member, IEEE), EVA ANTONINO-DAVIU, (Member, IEEE),
AND MIGUEL FERRANDO-BATALLER, (Life Member, IEEE)
Antennas and Propagation Laboratory (APL), iTEAM, Universitat Politècnica de València, 46022 Valencia, Spain
Corresponding author: Jaime Molins-Benlliure (jaimoben@iteam.upv.es)

ABSTRACT A novel methodology based on the sectorization of multiple-port cavities with azimuthal symmetry into sector unit cells is presented to design 5G multiple-input multiple-output (MIMO) sub-6 GHz antennas. The methodology divides an N-port cavity antenna into N unit cells and predicts the performance of the N-port design with the analysis of two adjacent cells. This approximation reduces the time and complexity of the simulation of cavity antennas with a high number of ports. For the theoretical justification, cavity mode analysis of a closed cavity and characteristic modes analysis of open and sector cavities is addressed. With the use of the proposed methodology, five different cavity designs with circular, square, hexagonal, octagonal, and saw-tooth geometries are presented in this article. In addition, the fabrication of the 4-port circular shape design and its MIMO performance is also studied. Results show an impedance bandwidth of 130% (1.27-6 GHz), and an envelope correlation coefficient (ECC) lower than 0.1.

INDEX TERMS 5G antenna, MIMO antenna, sub 6-GHz, wide-band antenna, 5G MIMO access point.

I. INTRODUCTION

The 5th generation wireless system (5G) was developed to satisfy the new requirements in terms of data rate, latency, efficiency, and reliability [1], [2] due to the enormous growth of data traffic in the current all-connected era. The 5G NR frequency bands are composed of the frequency range one (FR1) working at the so-called sub-6 GHz bands and the frequency range two (FR2), which cover the millimeter wave bands. The early deployment of the 5G is currently supported by the sub-6 GHz bands (FR1) due to the compatibility with the 2G/3G/4G infrastructure. The frequency bands which have received the most attention worldwide are the n77 (3.3-4.2 GHz), the n78 (3.3-3.8 GHz), and the n79 (4.4-5 GHz) bands.

This new scenario has raised the interest in multiple antennas solutions for 5G sub-6 GHz applications. One of the most relevant features for providing high data rates is the multiple-input multiple-output (MIMO) technology. In recent

The associate editor coordinating the review of this manuscript and approving it for publication was Prakasam Periasamy.

publications, there has been an enormous growth on the interest about MIMO compatible designs in size-limited devices for smartphones applications [3], [4], [5], [6], [7], medical applications [8] and for access point applications [9]. The coexistence of several antennas in size-limited scenarios produce highly coupled radiating elements, degrading their performance. Isolation techniques are widely used to cope with coupling issues, such as in [10] where a slotted stub is used to increase to 20 dB the isolation of two ultra wide-band stepped-shaped antennas ranging from 2 to 13.8 GHz. In [11] a transmission-line-based decoupling method is presented to increase 16-20 dB the isolation between co-polarized elements for a MIMO antenna array working at 2.4 GHz. In addition, an isolation structure is presented in [12] increasing 10-15.1 dB the isolation between elements providing connection to the n78 band for smartphone applications.

The 5G infrastructure will include indoor access points [13] to guarantee the 5G connection standards at indoor environments with poor signal levels. Most of the solutions are based on dual-polarized antennas due to its orthogonal and low correlated radiation patterns which is

the key parameter for the correct performance of MIMO antennas. A recent multi-band design [14] proposes a triple band with a dual-polarized antenna working at 5G n78 band and also providing 2G/3G/4G connection at 0.7-0.96 GHz and 1.7-3 GHz. Two dual-band dual-polarized solutions are detailed in [15] and [16] with the use of an AMC reflector [15] operating at n78/n79 bands with an isolation of 20 dB and a second solution with the use of crossed monopoles [16] operating at n78 and 1.55-2.75 GHz bands. In addition, a dual-band antenna is presented in [17] based on a slotted microstrip patch and two monopoles working at 0.8-9.6 GHz and 1.7-2.7 GHz obtaining an isolation of 18 dB. Lastly a 3-D printed crossed dipoles are presented in [18] providing service to n77/n78/n79 bands with 18 dB isolation.

When a higher number of ports is required, different arrangement of radiators are proposed for obtaining polarization diversity. Regarding 3-port wide-band solutions, a tripolarized antenna composed by a monopole-equivalent structure and two crossed stepped dipoles is presented in [19] operating at n77/n78 bands obtaining 30 dB isolation and 85% total efficiency. In addition, a 3-port equilateral triangular patch antenna working at 3.3-4.2 GHz band is analyzed in [20] with 82% total efficiency and 15 dB isolation. Concerning to 4-port solutions, two antennas are proposed in [21] and [22], with a single-patch based on quasi $TM_{1/2,1/2}$ mode ranging at 3.3-4.5 GHz band (15 dB isolation and 80% total efficiency) and with an annular-ring patch [22] with an impedance bandwidth ranging at 3.3-5 GHz (16.5 dB isolation and 84% total efficiency). A 6-port wide-band solution is presented in [23] with six uncorrelated waves using a circular patch antenna with 6 feedings and ranging from 3.1 to 7.2 GHz with 20 dB isolation and 85% of total efficiency.

The tendency of increasing the number of ports has led to complex designs with time and memory-consuming simulations. In array applications, Floquet theory proposes a methodology that studies the behavior of a periodic structure with a Cartesian coordinates system-based symmetry, analyzing only a unit cell simplifying the simulation process. Recent articles apply Floquet theory for the design of arrays [24], reflect-arrays [25], [26] and meta-surfaces [27]. In this paper, we propose a novel methodology based on polar coordinate system symmetry and benefits from the azimuth periodicity of the field distributions. Cavity modes and characteristic modes are used for the analysis of a closed and open circular coaxial cavity and different angle sectors. Characteristic modes analysis is introduced for the study of open cavities, which can not be analyzed by the classical theory of cavity modes.

In a previous article [28], the authors proposed a methodology based on characteristic modes to decouple with an x-shape block a 4-port cavity antenna with isolation issues. In this article, a different methodology is proposed for the design of similar N-port cavity antennas with a sector unit cell approximation. The proposed methodology guarantees that the analysis of two adjacent cells is enough for predicting the performance of an N-cell antenna, simplifying the designing

process and reducing the time of simulations. For designs with a higher number of ports, the decrease factor is considerable, converting the proposed methodology in a proper candidate for the simplification of the design of MIMO antennas. The novelty of this article leans on the proposed methodology, which has been successfully applied for the design of a 4-port circular open-cavity, a 4-port square open cavity, a 6-port hexagonal open cavity, an 8-port octagonal open cavity, and an 8-port teeth-saw open cavity. For the octagonal design, the use of the proposed methodology reduces their simulation time by a factor of 26. The 4-port circular open-cavity has been fabricated to demonstrate the viability of the methodology, and a MIMO compatibility study has also been provided with the calculation of the channel capacity and the envelope correlation coefficient (ECC).

The paper is organized as follows: In Section II, the study of the first cavity modes of a closed coaxial cavity and the characteristic modes analysis of an open coaxial cavity and its sectorization is addressed. The study focuses on the effect of reducing an open cavity into different angle sectors providing information about the modes which are present and the modes which are filtered. In Section III, the sector-unit cell methodology is presented, and a coaxial four-port design is analyzed for demonstration. Simulated and fabricated results are presented, including a MIMO system performance evaluation. In addition, three more designs are detailed with a systematic design strategy with regular polygon geometry cavities (square, hexagonal and octagonal) with the use of the sector unit cell methodology. In Section IV, an 8-port saw-tooth design with the use of the sector unit cell methodology with x-axis replication is analyzed. Finally, Section V exposes the conclusion of the paper.

II. COAXIAL CAVITIES ANALYSIS

In this section, the analysis of a closed coaxial cavity, an open cavity, and 1/2, 1/4, 1/6, and 1/8 open cavity sectors is addressed. Fig. 1(a) shows the coaxial closed cavity, that from now on will be denominated as the coaxial cavity. Fig. 2(a) presents the open coaxial cavity and its sectors. For the sake of comparison, they all have dimensions of r1=108.5 mm, r2=43.8 mm, and h1=34.2 mm, and the only difference is that the closed cavity has a top cover enclosing the structure and the open cavity has not.

Closed cavities are described in the electromagnetic literature through the use of cavity modes, and the electric and magnetic fields have been derived for canonical geometries [29] including the coaxial cavity, which is analytically described in [30]. On the contrary, open cavities are not analytically described, so we propose the use of characteristic mode analysis to analyze open cavities and sectors. In the following subsections, both analyses are addressed.

A. CAVITY MODES ANALYSIS OF A CLOSED COAXIAL CAVITY

In this subsection, the first five modes of a coaxial cavity (Fig. 1(a)) are analyzed. In cavity resonators, a three-symbol
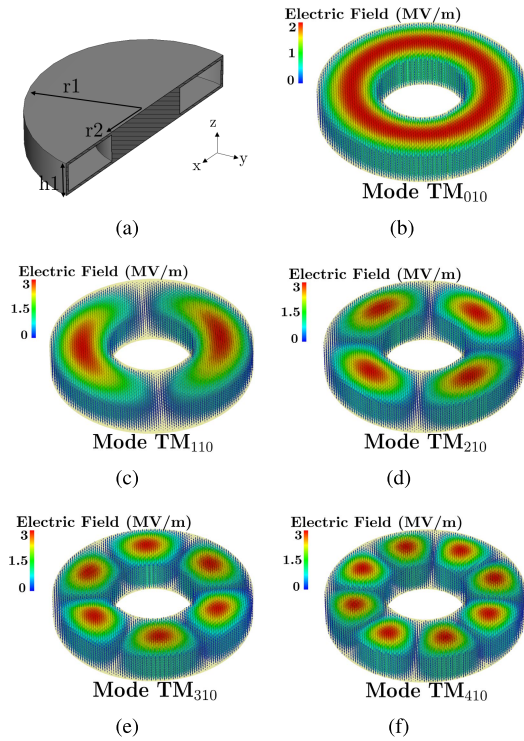
FIGURE 1. a) Section View of the coaxial cavity. Electric Field distribution of b) Mode TM_{010} c) Mode TM_{110} d) Mode TM_{210} e) Mode TM_{310} and f) Mode TM_{410}.

subscript is required (*mnp*) to describe both transverse (*mn*) and longitudinal (*p*) variations. In this case, the z-axis defines the longitudinal variation and has been settled as the direction of propagation.

The aim of the analysis is to check the azimuthal periodicity and symmetry of the first modes in order to divide the whole cavity into several sectors. The sector subdivision would simplify the analysis and simulation of a multiple-fed cavity-based design and would provide valuable information about the number of independent ports and the required type of excitation.

Fig. 1 depicts the analyzed coaxial cavity with r1=108.5 mm, r2=43.8 mm and h1=34.2 mm and the electric field distribution of the first resonant modes of the cavity: Modes TM_{010}, TM_{110}, TM_{210}, TM_{310} and TM_{410}. The azimuth variation of the electric fields, except of TM_{010} (which has no variation), has a sinusoidal behaviour defined by $\sin(\phi)$-TM_{110}, $\sin(2\phi)$-TM_{210}, $\sin(3\phi)$-TM_{310} and $\sin(4\phi)$-TM_{410}. The radial variation is equivalent in all of them.

With an inspection of the field distributions, it can be observed a division into N sectors depending on the azimuth variations of the electric field. For Mode TM_{110} two sectors are obtained, for mode TM_{210} four sectors, for mode TM_{310} six sectors and for TM_{410} eight sectors. The coaxial cavity could be segmented into N sectors, cutting the cavity through the maximums of electric field (colored in red) and applying a condition of open-circuit. All the fields distribution of the

modes are present if one of the N sectors is analyzed independently. This strategy would simplify the design process for multiple-port open cavities, whose simulation is time-demanding, especially when N is high. Since open-cavities cannot be described by cavity modes, in the following section, we turn to a characteristic modes analysis.

where $\vec{J}_n$ is the n_{th} real eigenvector (characteristic current) and λ_n is the n_{th} eigenvalue. [X] and [R] are the imaginary and real part of the generalized impedance matrix of the structure [Z].

B. CHARACTERISTIC MODES ANALYSIS (CMA) OF AN OPEN CAVITY AND ITS SECTOR SUBDIVISION

Open cavities have different boundary conditions than closed cavities, and the information regarding modes is not detailed in the available literature. We propose the use of characteristic modes analysis which is a proper approach for the analysis of an open coaxial cavity.

The Theory of Characteristic Modes (TCM) [31], [32] provides a basis set of currents on a structure with an arbitrary geometry, which exhibits orthogonal radiation properties. It provides a physical interpretation of the radiating mechanisms of the structure and helps to determine the optimum feeding configuration. Characteristic modes are calculated from the generalized impedance matrix of a structure [Z] (calculated using the Method of Moments (MoM)) and the resolution of the following eigenvalue problem:

$$[X]\vec{J}_n = \lambda_n[R]\vec{J}_n \qquad (1)$$

Eigenvalues (λ_n) are frequency-dependent and provide radiation information about the associated current mode. The mode stores electric energy (capacitive mode) when λ_n is negative and magnetic energy (inductive mode) when λ_n is positive. When $\lambda_n = 0$, the mode is at resonance. Different modal attributes for the physical interpretation of the eigenvalues have been proposed [33], [34]. In this paper, the characteristic angle (α_n) has been selected for the analysis, and it is derived as follows:

$$\alpha_n = 180° - \tan^{-1}(\lambda_n) \qquad (2)$$

When the mode is at resonance $\lambda_n = 0$, $\alpha_n = 180°$.

In this subsection, the characteristic modes analysis of an open coaxial cavity and its 1/2, 1/4, 1/6 and 1/8 sectors is addressed. Open coaxial cavity and sectors have equivalent r1, r2 and h1 (as depicted in Fig. 2(a)). The open coaxial cavity has equivalent dimensions as the closed cavity analyzed in the previous subsection but without the top cover enclosing the cavity. The decision of analyzing sectors with different sizes responds to the fact that the open cavity will be fed by N excitations and will be divided into N identical subdivisions or unit cells. The cavity then can be reinterpreted as a unit cell which is replicated N times with azimuthal periodicity. Commercial electromagnetic simulators are able to analyze unit cells with periodic boundaries when Cartesian axes of symmetry are used, but not when boundary conditions with
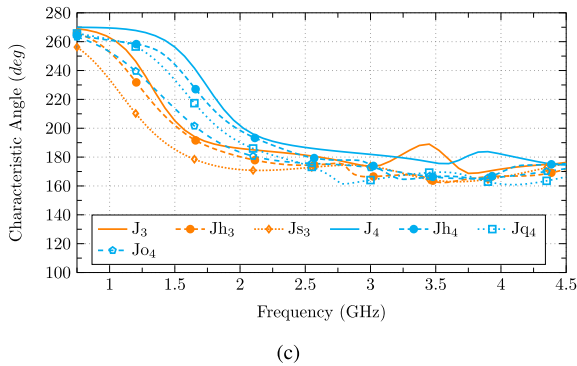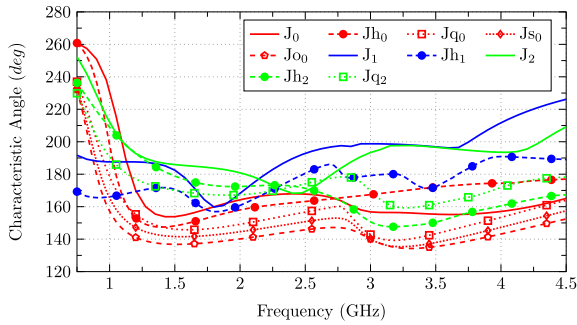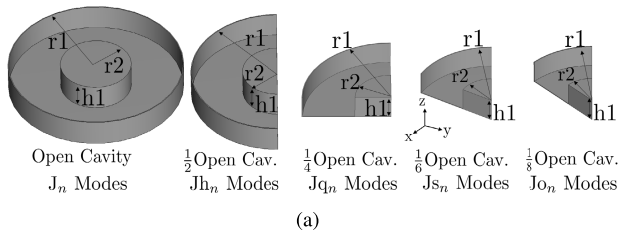
(a)

(b)

(c)

FIGURE 2. Open cavity and its 1/2, 1/4, 1/6 and 1/8 sectors: a) View, b) Characteristic angles from mode J_0 to mode J_2 and c) Characteristic angles of mode J_3 and J_4.

FIGURE 3. Modal field distribution at z=h plane of the open cavity and its 1/2, 1/4, 1/6 and 1/8 sectors from mode J_0 to mode J_4.

TABLE 1. Resonance frequency of the Modes.

	J_0	J_1	J_2	J_3	J_4
Cav.	1.2 GHz	1.52 GHz	2.05 GHz	2.55 GHz	3.25 GHz
1/2 Sec.	1.05 GHz	0.65 GHz	1.48 GHz	2.05 GHz	2.5 GHz
1/4 Sec.	1 GHz	✗	1.2 GHz	✗	2.3 GHz
1/6 Sec.	0.9 GHz	✗	✗	1.6 GHz	✗
1/8 Sec.	0.88 GHz	✗	✗	✗	2.15 GHz

azimuthal periodicity are needed. Since the desired periodicity conditions cannot be simulated, open boundary conditions are set along the symmetry planes, which cut the open cavity into sectors. The goal of this subsection is to analyze which modes are still present and which are filtered when the open cavity is reduced to different angle sectors.

Fig. 2(b) and Fig. 2(c) represent the characteristic angle of the five first resonant modes between 0.5-4.5 GHz of the open coaxial cavity and the equivalent modes after sectorization. The open coaxial cavity modes are denoted by J_n, the 1/2 sector modes by Jh_n, the 1/4 sector modes by Jq_n, the 1/6 sector modes by Js_n and the 1/8 sector modes by Jo_n. For their easier inspection, modes from J_0 to J_2 are represented in Fig. 2(b) and from J_3 to J_4 in Fig. 2(c). A shift on the characteristic angle of the sectors modes is observed due to the inductive effect produced by the currents flowing around their perimeter, and also, some modes vanish due to the modification of the structure. In general, the behaviour of the sectors conserved modes is similar to the original modes of the cavity.
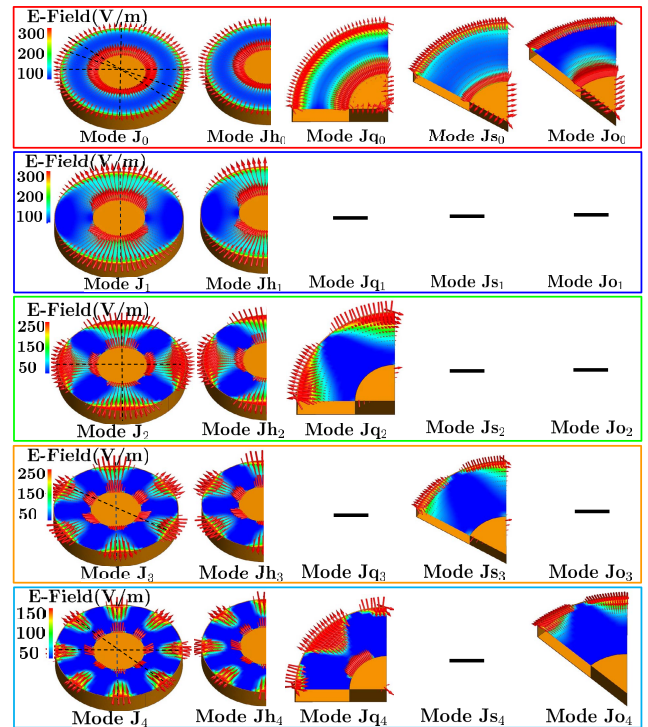
In Fig. 3 the modal electric field distribution at the corresponding resonance of the five first resonant modes of the open coaxial cavity and the equivalent modes of the 1/2, 1/4, 1/6, and 1/8 sectors is represented in z=h1=34.2 mm plane. Two types of modes are observed in Fig. 3, mode J_0 presents an electric field distribution with only radial variation. The rest of modes have both radial and azimuth variation in their associated radiated field. Since the electric field distribution of radial modes, like J_0, is constant in azimuth variation, these modes are always present in the cavity and in all the analyzed sectors. Modes with azimuth variation (J_1-J_4) exhibit sinusoidal field distribution along the perimeter of the cavity. They are at risk of vanishing if specific boundary conditions are not satisfied when the open cavity is reduced to a sector. Since an open circuit boundary condition is set through the lines of symmetry when sectors are created, modes must exhibit maximum field distribution where the cavity is cut. Lines of symmetry that satisfy the previously specified conditions are depicted in black dashed lines in Fig. 3. Definitely, if the cavity is split through the dashed lines, the mode will still be present in the created sector.
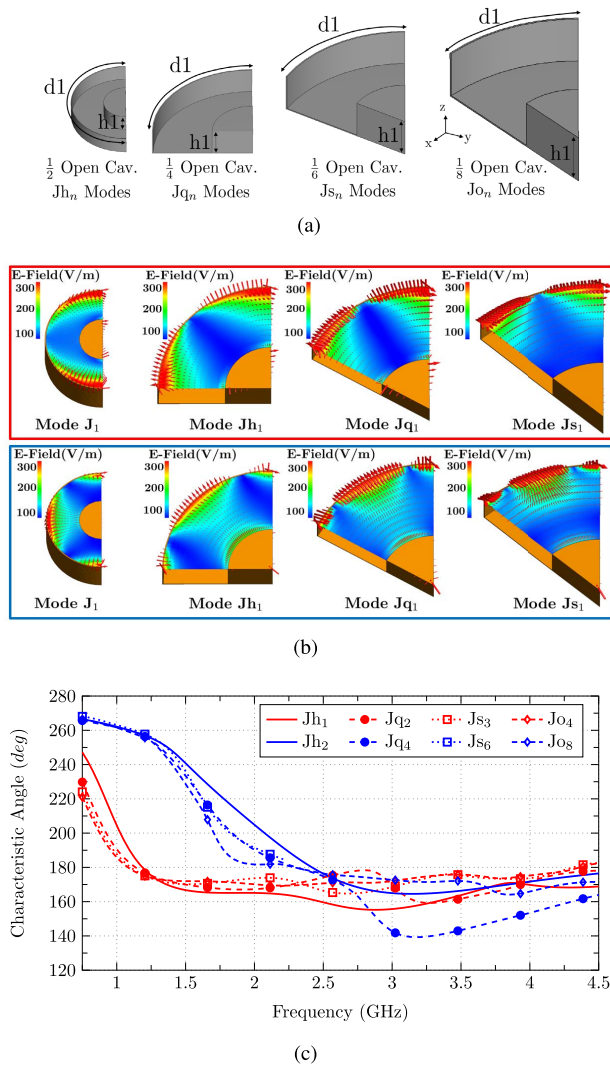
FIGURE 4. a) View of 1/2, 1/4, 1/6 and 1/8 sectors with equivalent arc length d1, b) Modal field distribution at z=h plane of the first two resonant modes of the analyzed sectors, and c) Characteristic angle of analyzed sectors.

According to this analysis, it can be stated that modes with only radial variation will always be present when sectorization is applied. On the contrary, azimuthal variation modes are filtered depending on the size of the sector. For the 1/2 sector, all the modes are present except for the degenerated modes. For the 1/4 sector, modes with $\sin(2n\phi)$ variation (n=1,2,3...) are present. 1/6 sector conserves $\sin(3n\phi)$ variation modes and 1/8 sector presents $\sin(4n\phi)$ variation modes. In conclusion, azimuthal variation modes will be present when sectorization of 1/N sector is applied if an electric field distribution of $\sin(\frac{N}{2}n\phi)$ for n=0,1,2... is satisfied in the cavity.

C. CMA OF SECTORS WITH EQUIVALENT ARC LENGTH

In the previous analysis, the open cavity has been reduced to different angle sectors with constant r1 and r2 dimensions. The analysis proposed in this subsection studies the 1/2, 1/4,

1/6, and 1/8 sectors with equivalent arc length (d1) and heigh (h1) of open cavities with different dimensions (different r1 and r2).

The motivation of the analysis responds to the fact of the future inclusion of feeding in the centre of the arc (d1) of each sector (sector unit cell), creating an N-port design if the sector unit cell is replicated N times. Distance d1 should guarantee a minimum distance between ports to avoid coupling ($\lambda/2$ at f_{min} approximately) and also defines the resonance frequency of the azimuthal modes. If distance d1 between ports is respected, the size of the perimeter of the cavity will be defined by N×d1. The higher N is, the higher the cavity size is and, the first modes will resonate at lower frequencies. The operating bandwidth will not be defined by the first resonating modes of the cavity but by the bandwidth of the excitation. The excited modes of high N cavities will be higher-order modes of the cavity because the first modes are far from the frequency which the feeding is operative.

In this study 1/2 (N=2), 1/4(N=4), 1/6(N=6) and 1/8(N=8) sectors of Fig. 4(a) with equivalent d1 are analyzed. The first two azimuthal resonating modes of the sectors are studied by representing the field distribution at resonance (Fig. 4(b)) and the characteristic angles (Fig. 4(c)). It can be observed that modes are resonant at approximately the same frequency (because d1 is equivalent), but modes come from different order modes of the complete cavity. It is then confirmed that if the cavity is scaled up with N×d1, there is always a mode that will be excited that comes from a different order mode of the complete cavity depending on N. The cavity size will not matter because d1 is respected and first modes (for high values of N) resonate at a frequency out of the bandwidth which the feeding is operative. The study confirms the conservation of the modes if d1 is respected.

III. SECTOR UNIT CELL METHODOLOGY

In this section, the information obtained from the previous analysis is used to present a sector unit cell methodology. This methodology predicts the performance of an N-port cavity-backed antenna by the analysis of only two of the N unit cells in which the antenna is divided.

In Section II, the modes of the coaxial open cavity and different angle sectors have been obtained. It has been demonstrated that radial modes are always present in both designs, but azimuth modes are filtered if certain boundary conditions are not satisfied when sectorization is applied.

Taking advantage of the obtained information regarding the conservation of the modes, we propose to feed an open cavity by N excitations arranged in a symmetric fashion and divide the whole design into N sectors unit cells. The new subdivision is called the sector unit cell and is composed of a sector of the cavity fed in the centre of the arc length by a T-shaped monopole.

The goal of the methodology is to simplify the analysis of the N-port design to the study of only a sector unit cell for impedance matching information and the study of two adjacent unit cells for the study of isolation. In previous
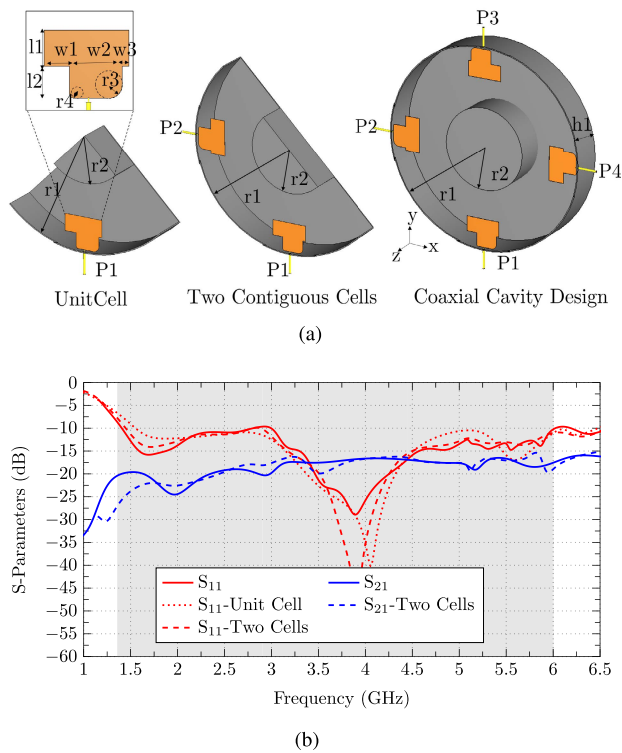
FIGURE 5. Unit cell, two contiguous cells and the open coaxial cavity antenna: a) Overall view and b) S-parameters.

TABLE 2. Dimensions of the circular 4P cavity design (unit: *mm*).

r1	r2	r3	r4	h1	w1	w2	w3
107.5	44	5.7	2	33	11.2	23.1	2.9

papers, coaxial cavities have been used due to their capacity to isolate faced ports exhibiting their minimum isolation level between contiguous ports. This feature allows to guarantee that all ports of the design are isolated if two contiguous ports are decoupled. Sector unit cell methodology benefits from this feature and guarantees a good isolation performance only by analyzing two contiguous unit cells.

The methodology leans on the fact that a minimum distance d1 (arc length of the unit cell) should be close to $\lambda/2$ at f_{min} to guarantee minimum isolation between adjacent ports. Since the perimeter of the cavity is obtained with N×d1, modes of the cavity from different order but with the same field variation at the unit cell are excited. The excitation consist of a wideband T-shaped monopole whose f_{min} is set by the $\lambda/4$ path between short (coaxial feeding point) and the open circuit (top edge of the monopole). The height of the cavity will be optimized due to its effect on the input impedance of the monopoles. Its value will be always constrained by a minimum of $\lambda/4$ and a maximum of $\lambda/2$ at the central frequency of the operating bandwidth.

In this section, two different cavity geometries are studied with the use of the sector unit cell methodology, a first subsection for the design of circular cavities and a second subsection
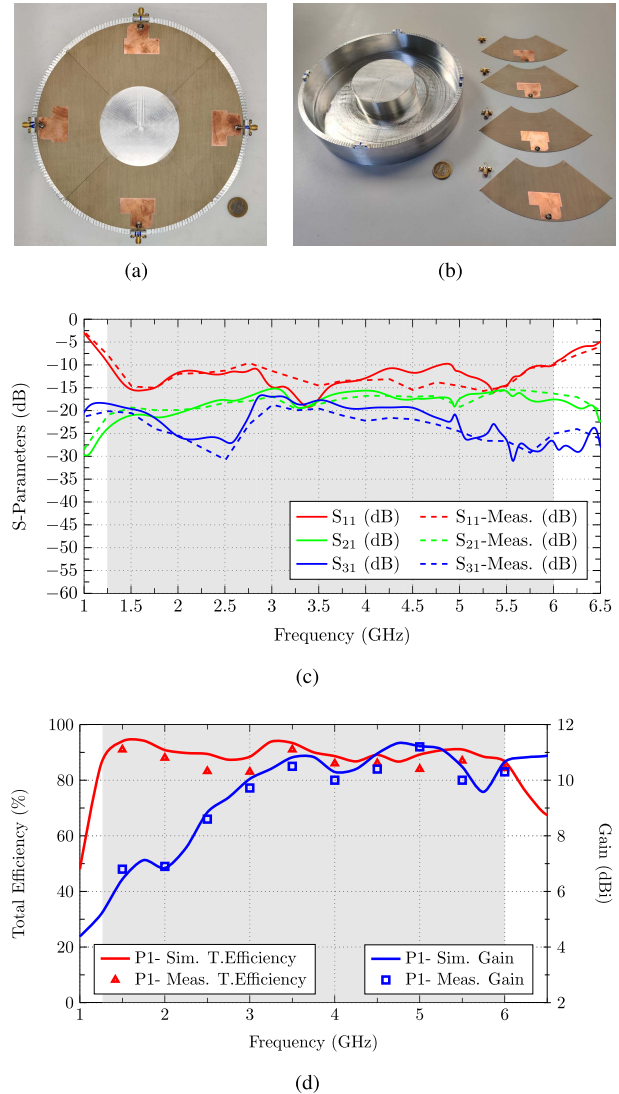

FIGURE 6. a) Front view of the Fabricated Antenna b) Dissembled antenna and c) S-parameters and d) Total efficiency and Gain of Port1.

for the design of regular polygon geometry cavities. For demonstration, a wideband 4-port circular coaxial cavity, a 4-port square coaxial cavity, a 6-port hexagonal coaxial cavity, and an 8-port octagonal coaxial cavity have been designed with the use of the proposed methodology. This designing method decreases the time and complexity of the design and simulation of multiple-fed open cavity solutions, especially when the number of ports is high.

A. DESIGN OF A CIRCULAR 4-PORT CAVITY WITH THE SECTOR UNIT CELL METHODOLOGY

In this subsection, the sector unit cell methodology is used for the design of a 4-port circular open cavity. The four excitations are placed in a symmetric and orthogonal fashion around the cavity. The number of unit cells is N=4, and they are composed of a quarter of the cavity and a T-shaped monopole.

The methodology is summarized at Fig. 5(a). The first stage of the methodology is based on the optimization of the dimensions of the unit cell in terms of matching. At the second stage, two unit cells are analyzed, and the dimensions are slightly modified, if needed, to guarantee a minimum isolation level of 15 dB. Finally, at the third stage, the whole design with all unit cells together is simulated to guarantee the correct performance of the antenna. The optimized dimensions of the design are detailed in table 2, resulting in a cavity with a height h = $\lambda/7$ for f_{min} and a distance between ports higher than d1 = $\lambda/2$ to guarantee 15 dB of isolation level.

In Fig. 5(b), the S-parameters computed for the three stages are depicted, including the reflection coefficient (S_{11}(dB)) and the coupling between contiguous unit cells (S_{21}(dB)). Solid lines represent the results of the coaxial open cavity design, densely dashed curves of the Unit Cell, and dashed curves the two adjacent cells. The reflection coefficient is slightly shifted to lower frequencies for the two unit cells and coaxial open cavity design due to the wider area where the currents can flow. Isolation is not in a good agreement between 1-1.5 GHz, but in this band, the coupling level is not critical. The S-parameters represented in Fig. 5(b) show highly correlated results of matching and isolation between the unit cells and the complete design confirming the reliability of the methodology of designing N-port antennas with the analysis of sector unit cells.

The fabrication and the MIMO performance of the 4-port coaxial antenna are presented next in order to prove the accuracy of the methodology.

1) RESULTS AND FABRICATION

The 4-port coaxial circular cavity antenna has been fabricated using a Rogers R04003C PCB (ϵ_r = 3.55, $\tan\delta$ = 0.0027 and thickness t = 0.6 mm) for supporting the four T-shaped monopoles (Fig. 6(a)) on the aperture of cavity. The cavity has been milled from a solid aluminum cylinder. Four coaxial ports have been screwed and welded to the four monopoles. Fig. 6(b) depicts the disassembled design for its correct inspection. The simulated (solid curves) and the measured (dashed curves) of the S-Parameters are represented in Fig.6(c) with an impedance bandwidth ranging from 1.25 GHz to 6 GHz. The isolation is higher than 15 dB in all the band (S_{21}(dB)= S_{41}(dB) and S_{31} in Fig.6(c)). Both are obtained with the use of the Rogers PCB represented Fig. 6(c). The S-parameters slightly differ from the results of Fig. 6(b) due to the inclusion of the Rogers PCB. In addition, the total simulated and measured total efficiency and gain are represented in Fig. 6(c) with a good agreement between simulated and measured results. Results show a measured efficiency higher than 82% and an average gain of 8 dBi.

Regarding the radiation patterns, Fig. 7 depicts measured and simulated patterns in XZ plane ($\phi = 0°$) and YZ plane ($\phi = 90°$) at 1.5 GHz (Fig. 7(a)), 3 GHz (Fig. 7(b)), 4.5 GHz (Fig. 7(c)) and 6 GHz (Fig. 7(d)). When the frequency is low, the radiation pattern is composed of a single lobe. When the frequency increases, the radiation pattern is slightly
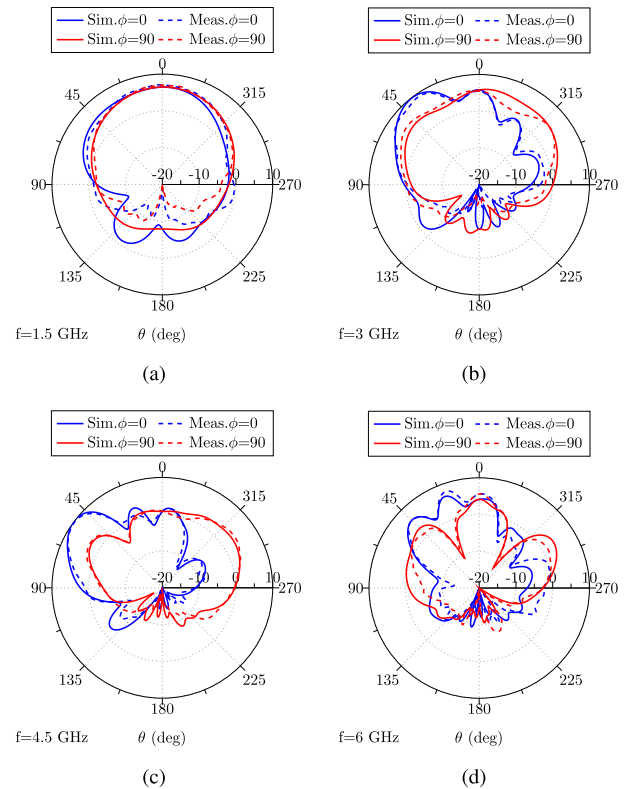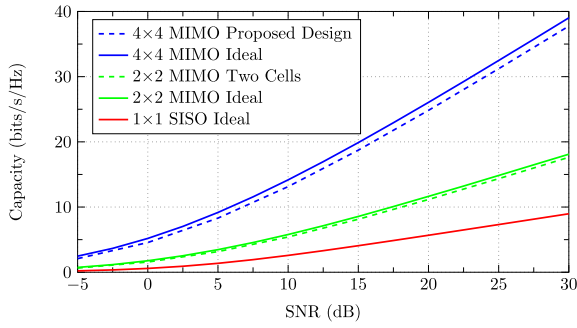

FIGURE 7. Simulated (solid) and Measured (dashed) radiation pattern of P1. Plane $\phi = 0°$ (blue) and $\phi = 90°$ (red) at: a) f=1.5 GHz, b) 3 GHz, c) 4.5 GHz and d) 6 GHz.

disturbed, and side lobes appear. The antenna keeps a unidirectional radiation pattern in all the operating band.
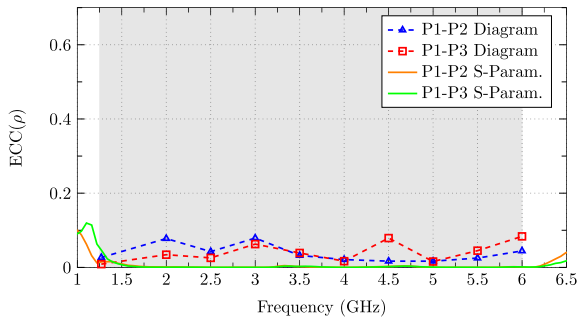
2) MIMO SYSTEM PERFORMANCE

This subsection addresses the performance of the proposed 4-port coaxial circular cavity antenna (composed of 4 unit cells) and a half of the design (antenna composed of two contiguous cells) in a 4×4 and 2×2 MIMO systems, respectively, taking into consideration the propagation channel. For the study, the channel capacity in the presence of mutual coupling [35] and the envelope correlation coefficient (ECC) in a scenario with isotropic scattering (described by a uniform distribution) is calculated. The proposed antenna, due to its wide-band behavior, obtains a minimum isolation level of 15 dB. In order to guarantee that the MIMO performance is not compromised by this parameter, the ideal (no coupling) channel capacity and the channel capacity obtained with the use of the proposed antenna at the lowest isolation level frequency (f=3.1 GHz) are compared.

The channel capacity [35] is calculated with the use of 4 uncorrelated antennas as transmitting antennas, and the four receiving antennas are the four antennas of the proposed design. It is assumed isotropic scattering environment and perfect channel state information (CSI) for the receiver but not for the transmitter. Hence, the ergodic capacity can be derived as (3) [35] where I is the 4×4 identity matrix, $\overline{\gamma}_0$

(a)

(b)

FIGURE 8. a) Channel Capacity and b) Envelope correlation coefficient (ECC).

FIGURE 9. Unit cell equations and the obtained angles and dimensions for a square(N=4), hexagonal (N=6) and octagonal (N=8) open cavity designs unit cells.

TABLE 3. Dimensions of the initial design (unit: *mm*).

	Lx	rx	Hx	bx	r3x	r4x	w1x	w2x	w3x
Square	138	97.5	28.5	36	5.8	2	13.7	26.6	0.9
Hex.	136.5	136.5	38.4	40	5	1.6	9.6	19.8	2.5
Oct.	129.7	168.5	40	50	5.1	1.7	10	20.6	2.6

the SNR, R the correlation matrix of the receive antenna and H_w the spatially white MIMO channel with independent and identically distributed (i.i.d) complex Gaussian entries. H_w^H denotes hermitian of H_w.

$$C = E \left\{ \log_2 \left[\det \left(I + \frac{\overline{\gamma_0}}{2} R H_w H_w^H \right) \right] \right\} \quad (3)$$

Fig. 8(a) represents the calculated channel capacity with 100000 simulated 4×4 MIMO channels using as receiving antennas the proposed design (dashed blue curve), an ideal design without coupling (blue curve). The same process is repeated for a 2×2 MIMO system setting the two contiguous cells as receiving antennas and two uncorrelated antennas as the transmitting ones and calculating the capacity (dashed green curve). For the sake of comparison, the capacity of a 2×2 ideal MIMO system (green curve) and an ideal 1×1 SISO system (red curve) are also depicted. Results show similar capacities from the ideal case to the one using the proposed antenna. With these results, the good performance of the design is confirmed even in the frequency band with higher coupling levels. It can also be observed the capacity gain (x4) with the use of a 4×4 MIMO system and (x2) with the 2×2 MIMO system instead of a 1×1 SISO system.

The correlation coefficient (ECC) correlates two radiation patterns depending on the frequency and the propagation conditions and it is defined by (4). In (4) $g_1(\Omega)$ and $g_2(\Omega)$ details the two radiation patterns, $\Omega = (\theta, \phi)$ describes the solid angle of arrival and $Pa(\Omega)$ represents the dyadic power of the angular spectrum of the incident field
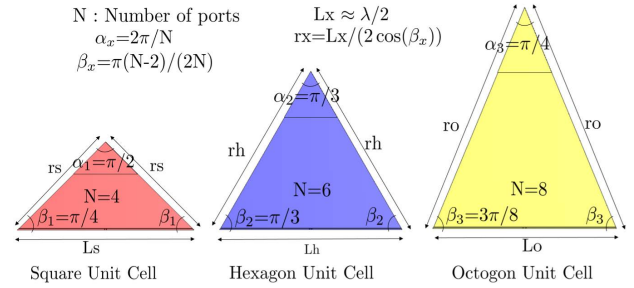
described by different angular distributions (Uniform, Gaussian, Laplace) [36]. ECC values lower than 0.5 are expected for uncorrelated radiation patterns [37]. In this article, the ECC is calculated in an ideal scenario with isotropic scattering. Hence $Pa(\theta,\phi)$ is assumed to be described by a uniform distribution ($Pa(\theta,\phi)= 1$), (4), as shown at the bottom of the next page.

The ECC can also be calculated with an approximation through the use of the S-parameters of the antenna (5) [38] assuming a scenario with isotropic scattering.

$$\rho = \frac{|S_{11}^* S_{12} + S_{21}^* S_{22}|^2}{(1 - (|S_{11}|^2 + |S_{21}|^2))(1 - (|S_{22}|^2 + |S_{12}|^2))} \quad (5)$$

Fig. 8(a) depicts both the calculated ECC with measured radiation patterns(dashed curves) and also with the S-parameters approximation (solid curves). Results confirm ECC values are always lower than 0.1 for the calculation between P1-P2 and P1-P3. Due to the symmetry of the design, only these two calculations are required.

After the analysis of the channel capacity and the ECC results, it can be stated that the proposed antenna is compatible and a good candidate for MIMO applications.

B. DESIGN OF REGULAR POLYGONS CAVITIES WITH THE USE OF THE SECTOR UNIT CELL METHODOLOGY

In this section, the Unit Cell Methodology is applied for the design of coaxial cavities with regular polygon geometry. In the centre of each face of the polygon, a feeding is connected; hence, the number of ports N of the designs is equal to the number of faces of the polygon. A design with four ports has then a square shape, six ports hexagonal, eight ports octagonal, and so on. The distance d1, which describes the arc sector of the unit cell of the circular design and the distance between ports, in these designs, it is described more intuitively by the side length (Lx) of the regular polygon shape.
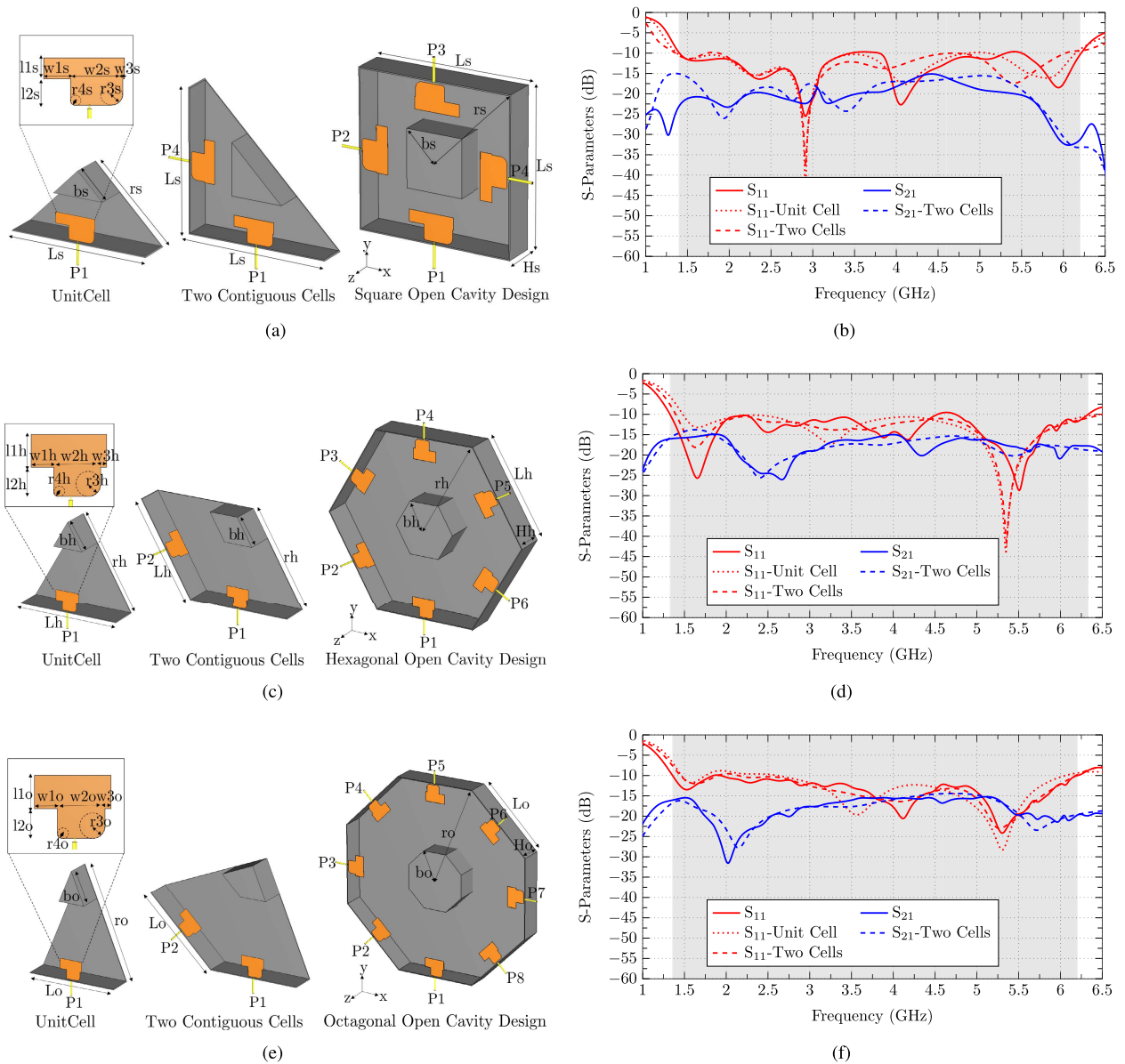
FIGURE 10. Scheme of the sector unit cell methodology for: a) square open cavity design, c) hexagonal open cavity design and e) octagonal open cavity design. S-parameters of the unit cell, two contiguous cells and complete design of b) square open cavity design, d) hexagonal open cavity design and f) octagonal open cavity design.

A systematic design process is presented for the optimization of the unit cell of an N port design with regular polygon geometry. The equations detailed in Fig. 9 are meant to be used with unit cells of any regular polygon geometry. The distance between ports must be close to $\lambda/2$ at f_{min} to guarantee a minimum isolation level of 15 dB, hence $L_x \approx \lambda/2$. The

angles β_x of the base of the unit cell increases with N, and it is defined by $\beta_x = \pi(N\text{-}2)/(2N)$. The top angle α_x decreases with N, and it is defined by $\alpha_x = 2\pi/N$. In Fig. 9 the unit cell of an N=4 (square cavity-red), N=6 (hexagonal cavity-blue), and N=8 (octagonal-yellow) cavities are obtained with the use of the proposed equations.

$$\rho = \frac{\iint\limits_{4\pi} g_1^H(\Omega)Pa(\Omega)g_2(\Omega)\,d\Omega}{\sqrt{\iint\limits_{4\pi} g_1^H(\Omega)Pa(\Omega)g_1(\Omega)\,d\Omega \cdot \iint\limits_{4\pi} g_2^H(\Omega)Pa(\Omega)g_2(\Omega)\,d\Omega}} \qquad (4)$$
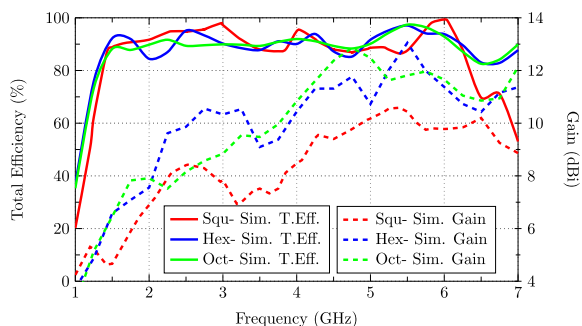
FIGURE 11. a) Simulated total efficiency and simulated gain of the square, hexagonal and octagonal designs.

With this information, it is simple and fast to optimize a unit cell of an N-port regular polygon geometry, no matter the number of N. This process limits the simulation and optimization process of the whole design to the time of optimizing a unit cell and checking the isolation with a contiguous cell.

In order to check the viability of the methodology, three examples are presented in Fig. 10 with square (N=4), hexagonal (N=6), and octagonal (N=8) geometries. The three unit cells have been optimized in terms of matching (S_{11}(dB)) at a first stage, including the monopole, and then, for isolation purposes, two contiguous unit cells have been analyzed. After these two studies, the whole design is simulated in order to check the correlation between the unit cell approximation and the whole design performance. The S-parameters of the three stages are represented for the three geometries, and only S_{11}(dB) and S_{21}(dB) are represented due to the symmetry of the design and also because contiguous ports show the lowest isolation levels. Results present a 4-port square open cavity, a 6-port hexagonal open cavity, and an 8-port octagonal open cavity with an impedance bandwidth of 126% (1.4-6.2 GHz), 130% (1.33-6.33 GHz) and 128% (1.36-6.2 GHz), respectively, with isolation always higher than 15 dB. Highly correlated results between the unit cell and the whole design confirm the viability of the methodology. Additionally, simulated total efficiency and gain are represented in Fig. 11 obtaining results higher than 82% of total efficiency.

IV. SECTOR UNIT CELL METHODOLOGY WITH X-AXIS REPLICATION. 8-PORT SAW-TOOTH DESIGN

All the designs analyzed so far are based on the unit cell methodology with the azimuth replication of a unit cell, creating closed cavity designs with canonical shapes. In this section, it is explored another way of designing cavity-based structures with the replication of the unit cell through the x-axis, obtaining a saw-tooth (linear array disposition) antenna (Fig 12(a)).

In this case, the obtained design is not symmetric, and it involves more complexity than the previous ones. The methodology has been only used for the matching information prediction (S_{11}(dB) dotted curve of Fig 12(b)). The unit
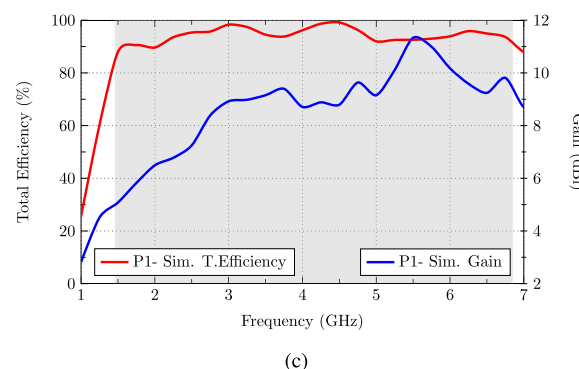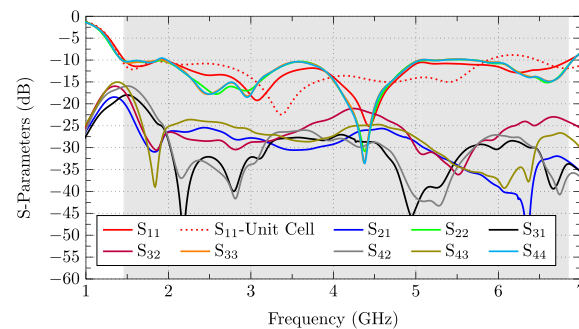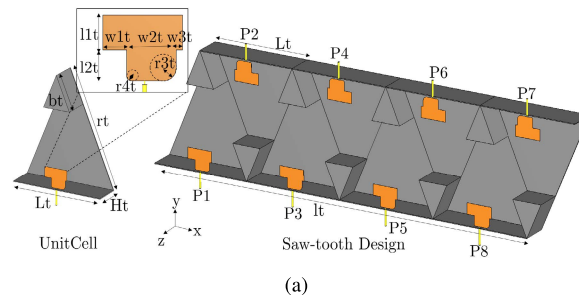

(a)

(b)

(c)

FIGURE 12. a) Scheme of the sector unit cell methodology for x-axis replication for the saw-tooth design, b) S-parameters of the unit cell, two contiguous cells and complete design and c) Port 1 simulated total efficiency and gain of the complete design.

TABLE 4. Dimensions of the saw-tooth design (unit: *mm*).

lt	Lt	rt	Ht	bt	r3t	r4t	w1t	w2t	w3t
555.5	138.8	180.45	35.9	50	5.1	1.7	9.5	22.3	1.5

cell has been obtained from the octagonal open coaxial design and has been slightly modified due to isolation problems in the saw-tooth design disposition. The separation between contiguous has been increased because the coupling between contiguous cells experienced higher coupling values when they were replicated through the x-axis. Fig 12(b) show the S-parameters of the saw-tooth design with an impedance bandwidth of 129% (1.46-6.85 GHz) and isolation higher than 15dB. Furthermore, simulated gain and total efficiency are represented in Fig 12(c) with values of an average 8 dBi gain and a total efficiency higher than 82%.

TABLE 5. Comparison table.

Ref.	BW (GHz)	BW (%)	Size (mm^3)	Isolation (dB)	N-Ports	T.Efficiency (%)
[14]	0.70-0.96 / 1.7-3 / 3.3-3.8	31 / 55.3 / 14	220×220×100	19	2	NA
[15]	3.14-3.83 / 4.4-5.02	19.8 / 13.2	79.6×79.6×10	20	2	NA
[16]	1.55-2.75 / 3.3-3.8	55.8 / 14	150×150×48	30	2	78
[17]	0.8-0.96 / 1.7-2.7	22 / 71.8	220×220×42	18	2	NA
[18]	3.5-5.1	37	27.2×27.2×17	18	2	NA
[19]	1.68-4.15	84.73	159.5×159.5×2.7	30	3	85
[20]	3.3-4.2	24	70×70×11.5	15	3	82
[21]	3.3-4.5	31	100×100×10	15	4	80
[22]	3.3-5	41	133×133×10	16.5	4	84
[23]	3.1-7.2	80	195×195×14	20	6	85
Square	**1.4-6.2**	**126**	**138×138×28.5**	**15**	**4**	**84**
Hexagonal	**1.33-6.33**	**130**	**219.5×219.5×38.4**	**15**	**6**	**82**
Octagonal	**1.36-6.2**	**128**	**284×284×28.2**	**15**	**8**	**84**
Saw-tooth	**1.46-6.85**	**129**	**555.5×166.6×35.9**	**15.1**	**8**	**82**
Circular	**1.27-6**	**130**	**190.5×190.5×33**	**15**	**4**	**82**

It is demonstrated that further distribution with different geometries can also be obtained with the replication of the unit cell, but only matching can be predicted. Isolation must be checked in the complete design due to the lack of symmetry of the structure. This way of replication of the unit cells offers a new disposition which increases the flexibility of the use of this methodology.

V. CONCLUSION

In this paper, a novel methodology based on the subdivision of an N-port cavity with radial symmetry into N sector unit cells has been presented for N-port MIMO antenna designs for 5G/Wi-Fi indoor access point applications. The methodology simplifies the design and simulation process thanks to the approach based on with the analysis of two contiguous cells. With the study of two contiguous cells, the performance of the N-port antenna can be predicted. For the physical insight justification of the methodology, a complementary cavity mode analysis of a close circular coaxial cavity and a characteristic mode analysis of a coaxial circular open cavity and its unit cell (1/4 of the open cavity) has been addressed. With the analysis, it has been demonstrated which modes are filtered due to the simplification of the cavity to the unit cell and which others remain. Radial modes and feeding modes are present, and modes with azimuth variation are filtered if a certain symmetry condition is not fulfilled.

Five designs of N-port open cavities with circular (N=4), square (N=4), hexagonal (N=6), octagonal (N=8), and teeth-saw (N=8) shapes have been successfully designed with the use of the proposed methodology. Matching and isolation correlation between the unit cell approximation and the complete design has been confirmed to be high, and the slight differences are due to the filtered modes when the reduction to a unit cell is applied.

The fabrication of the circular coaxial design with four ports has also been presented. Measurements and simulations exhibit good agreement with an impedance bandwidth (S$_{11}$(dB)< −10 dB) of 130% (1.27-6 GHz), isolation between ports higher than 15 dB. The channel capacity and ECC<0.1 have also been calculated, providing compatibility with a 4 × 4 MIMO system.

Simulated results of the square, hexagonal, octagonal and saw-tooth designs show an impedance bandwidth (S$_{11}$(dB)< −10 dB) of 126% (1.4-6.2 GHz), 130% (1.33-6.33 GHz), 128% (1.36-6.2 GHz) and 129% (1.46-6.85 GHz) respectively. Isolation between ports is always higher than 15 dB because the minimum distance between ports of $\lambda/2$ is always respected. Additionally, Table 5 compares the features of the most relevant recent publications of MIMO access point antennas and the proposed designs, highlighting the impedance bandwidth, the size, the isolation, the number of independent ports and the total efficiency.

The proposed sector unit cell methodology introduces a great simplification of the simulation and design process and a systematic strategy for designing complex and time-demanding cavity-based designs with a high number of ports. As a reference, the simulation of the 8-port octagonal design takes 4h 0m 14s, the simulation of two unit cells 8m 57s and a unit cell 4m 6s in a computer with 16 GB of RAM and an Intel Core i7-8700 CPU. It is then justified the benefits of using the unit cell approximation methodology.

REFERENCES

[1] N. Zhang, P. Yang, J. Ren, D. Chen, Y. Li, and X. Shen, "Synergy of big data and 5G wireless networks: Opportunities, approaches, and challenges," *IEEE Wireless Commun.*, vol. 25, no. 1, pp. 12–18, Feb. 2018.

[2] M. Agiwal, A. Roy, and N. Saxena, "Next generation 5G wireless networks: A comprehensive survey," *IEEE Commun. Surveys Tuts.*, vol. 18, no. 3, pp. 1617–1655, 3rd Quart., 2016.

[3] H.-D. Chen, Y.-C. Tsai, C.-Y.-D. Sim, and C. Kuo, "Broadband eight-antenna array design for sub-6 GHz 5G NR bands metal-frame smartphone applications," *IEEE Antennas Wireless Propag. Lett.*, vol. 19, no. 7, pp. 1078–1082, Jul. 2020.

[4] Z. Ren, A. Zhao, and S. Wu, "MIMO antenna with compact decoupled antenna pairs for 5G mobile terminals," *IEEE Antennas Wireless Propag. Lett.*, vol. 18, no. 7, pp. 1367–1371, Jul. 2019.

[5] S. Saxena, B. K. Kanaujia, S. Dwari, S. Kumar, H. C. Choi, and K. W. Kim, "Planar four-port dual circularly-polarized MIMO antenna for sub-6 GHz band," *IEEE Access*, vol. 8, pp. 90779–90791, 2020.

[6] D. Serghiou, M. Khalily, V. Singh, A. Araghi, and R. Tafazolli, "Sub-6 GHz dual-band 8×8 MIMO antenna for 5G smartphones," *IEEE Antennas Wireless Propag. Lett.*, vol. 19, no. 9, pp. 1546–1550, Jul. 2020.

[7] X.-T. Yuan, W. He, K.-D. Hong, C.-Z. Han, Z. Chen, and T. Yuan, "Ultra-wideband MIMO antenna system with high element-isolation for 5G smartphone application," *IEEE Access*, vol. 8, pp. 56281–56289, 2020.

[8] I. Elfergani, A. Iqbal, C. Zebiri, A. Basir, J. Rodriguez, M. Sajedin, A. D. O. Pereira, W. Mshwat, R. Abd-Alhameed, and S. Ullah, "Low-profile and closely spaced four-element MIMO antenna for wireless body area networks," *Electronics*, vol. 9, no. 2, p. 258, Feb. 2020.

[9] R. Hussain and M. S. Sharawi, "5G MIMO antenna designs for base station and user equipment: Some recent developments and trends," *IEEE Antennas Propag. Mag.*, vol. 64, no. 3, pp. 95–107, Jun. 2022.

[10] A. Altaf, A. Iqbal, A. Smida, J. Smida, A. A. Althuwayb, S. H. Kiani, M. Alibakhshikenari, F. Falcone, and E. Limiti, "Isolation improvement in UWB-MIMO antenna system using slotted stub," *Electronics*, vol. 9, no. 10, p. 1582, 2020.

[11] Y.-M. Zhang, S. Zhang, J.-L. Li, and G. F. Pedersen, "A transmission-line-based decoupling method for MIMO antenna arrays," *IEEE Trans. Antennas Propag.*, vol. 67, no. 5, pp. 3117–3131, May 2019.

[12] W. Jiang, Y. Cui, B. Liu, W. Hu, and Y. Xi, "A dual-band MIMO antenna with enhanced isolation for 5G smartphone applications," *IEEE Access*, vol. 7, pp. 112554–112563, 2019.

[13] F. Al-Turjman, E. Ever, and H. Zahmatkesh, "Small cells in the forthcoming 5G/IoT: Traffic modelling and deployment overview," *IEEE Commun. Surveys Tuts.*, vol. 21, no. 1, pp. 28–65, 1st Quart. 2019.

[14] A. Alieldin, Y. Huang, S. J. Boyes, M. Stanley, S. D. Joseph, Q. Hua, and D. Lei, "A triple-band dual-polarized indoor base station antenna for 2G, 3G, 4G and sub-6 GHz 5G applications," *IEEE Access*, vol. 6, pp. 49209–49216, 2018.

[15] Q. Liu, H. Liu, W. He, and S. He, "A low-profile dual-band dual-polarized antenna with an AMC reflector for 5G communications," *IEEE Access*, vol. 8, pp. 24072–24080, 2020.

[16] Z. Li, J. Han, Y. Mu, X. Gao, and L. Li, "Dual-band dual-polarized base station antenna with a notch band for 2/3/4/5G communication systems," *IEEE Antennas Wireless Propag. Lett.*, vol. 19, no. 12, pp. 2462–2466, Dec. 2020.

[17] Y. Zhao, C. Rakluea, T. Hongnara, and S. Chaimool, "A compact dual-broadband multiple-input multiple-output (MIMO) indoor base station antenna for 2G/3G/LTE systems," *IEEE Access*, vol. 7, pp. 82238–82245, 2019.

[18] Y. Li, C. Wang, H. Yuan, N. Liu, H. Zhao, and X. Li, "A 5G MIMO antenna manufactured by 3-D printing method," *IEEE Antennas Wireless Propag. Lett.*, vol. 16, pp. 657–660, 2016.

[19] S. X. Ta, D. M. Nguyen, K. K. Nguyen, C. Dao-Ngoc, and N. Nguyen-Trong, "A tripolarized antenna with ultrawide operational bandwidth," *IEEE Trans. Antennas Propag.*, vol. 68, no. 6, pp. 4386–4396, Jun. 2020.

[20] K. L. Wong and G. L. Yan, "Wideband three-port equilateral triangular patch antenna generating three uncorrelated waves for 5G MIMO access points," *IEEE Access*, vol. 10, pp. 893–899, 2021.

[21] K.-L. Wong, X.-Q. Ye, and W.-Y. Li, "Wideband four-port single-patch antenna based on the quasi-tm 1/2, 1/2 mode for 5G MIMO access-point application," *IEEE Access*, vol. 10, pp. 9232–9240, 2022.

[22] K. L. Wong, J. Z. Chen, and W. Y. Li, "Four-port wideband annular-ring patch antenna generating four decoupled waves for 5G multi-input–multi-output access points," *IEEE Trans. Antennas Propag.*, vol. 69, pp. 2946–2951, 2020.

[23] K.-L. Wong, Z.-W. Tso, and W.-Y. Li, "Very-wide-band six-port single-patch antenna with six uncorrelated waves for MIMO access points," *IEEE Access*, vol. 10, pp. 69555–69567, 2022.

[24] Y. Kim, H. Kim, I. Yoon, and J. Oh, "4 × 8 patch array-fed FR4-based transmit array antennas for affordable and reliable 5G beam steering," *IEEE Access*, vol. 7, pp. 88881–88893, 2019.

[25] M. E. Trampler, R. E. Lovato, and X. Gong, "Dual-resonance continuously beam-scanning X-band reflectarray antenna," *IEEE Trans. Antennas Propag.*, vol. 68, no. 8, pp. 6080–6087, Aug. 2020.

[26] E. Ozturk and B. Saka, "Multilayer Minkowski reflectarray antenna with improved phase performance," 2020, *arXiv:2009.12343*.

[27] K. Singh, M. U. Afzal, M. Kovaleva, and K. P. Esselle, "Controlling the most significant grating lobes in two-dimensional beam-steering systems with phase-gradient metasurfaces," *IEEE Trans. Antennas Propag.*, vol. 68, no. 3, pp. 1389–1401, Mar. 2019.

[28] J. Molins-Benlliure, E. Antonino-Daviu, M. Cabedo-Fabres, and M. Ferrando-Bataller, "Four-port wide-band cavity-backed antenna with isolating X-shaped block for sub-6 GHz 5G indoor base stations," *IEEE Access*, vol. 9, pp. 80535–80545, 2021.

[29] R. F. Harrington, *Time-Harmonic Electromagnetic Fields* (IEEE Press Series on Electromagnetic Wave Theory). New York, NY, USA: IEEE Press, 2001.

[30] M. K. Joshi, S. K. Vyas, T. Tiwari, and R. Bhattacharjee, "Optimal design of a coaxial cavity based on quality-factor maximization for high-power coaxial magnetron in *X*-band," *IEEE Trans. Plasma Sci.*, vol. 46, no. 3, pp. 503–510, Mar. 2018.

[31] R. F. Harrington and J. R. Mautz, "Theory of characteristic modes for conducting bodies," *IEEE Trans. Antennas Propag.*, vol. AP-19, no. 5, pp. 622–628, Sep. 1971.

[32] R. F. Harrington and J. R. Mautz, "Computation of characteristic modes for conducting bodies," *IEEE Trans. Antennas Propag.*, vol. AP-19, no. 5, pp. 629–639, Sep. 1971.

[33] M. Cabedo-Fabrés, "Systematic design of antennas using the theory of characteristic modes," Ph.D. dissertation, Antennas Propag. Lab (APL)-iTEAM, Univ. Politècnica de València (UPV), València, Spain, 2008.

[34] M. Cabedo-Fabres, E. Antonino-Daviu, A. Valero-Nogueira, and M. F. Batalle, "The theory of characteristic modes revisited: A contribution to the design of antennas for modern applications," *IEEE Antennas Propag. Mag.*, vol. 49, no. 5, pp. 52–68, Oct. 2007.

[35] X. Chen, S. Zhang, and Q. Li, "A review of mutual coupling in MIMO systems," *IEEE Access*, vol. 6, pp. 24706–24719, 2018.

[36] B. T. Quist and M. A. Jensen, "Optimal antenna radiation characteristics for diversity and MIMO systems," *IEEE Trans. Antennas Propag.*, vol. 57, no. 11, pp. 3474–3481, Nov. 2009.

[37] M.-Y. Li, Y.-L. Ban, Z.-Q. Xu, G. Wu, K. Kang, and Z.-F. Yu, "Eight-port orthogonally dual-polarized antenna array for 5G smartphone applications," *IEEE Trans. Antennas Propag.*, vol. 64, no. 9, pp. 3820–3830, Sep. 2016.

[38] S. Blanch, J. Romeu, and I. Corbella, "Exact representation of antenna system diversity performance from input parameter description," *Electron. Lett.*, vol. 39, no. 9, pp. 705–707, May 2003.

JAIME MOLINS-BENLLIURE (Student Member, IEEE) was born in València, Spain, in 1990. He received the bachelor's degree in telecommunications technology and services engineering and the master's degree in telecommunications engineering from the Polytechnic University of Valencia (UPV), València, in 2015 and 2017, respectively, where he is currently pursuing the Ph.D. degree in telecommunication engineering with the Instituto de Telecomunicaciones y Aplicaciones Multimedia (iTEAM), under a scholarship supported by the Spanish Ministry of Science and Innovation. He wrote his thesis under an Erasmus Scholarship with the Karlsruhe Institute of Technology (KIT), Karslruhe, Germany.

He was involved in a 5G Antenna Research Project Financed by Huawei Technologies OY Finland designing and fabricating antennas for 5G MIMO communication systems. He has submitted several papers in international and national conferences for the European Conference on Antennas and Propagation (EuCAP) and for the International Symposium on Antennas and Propagation and North American Radio Science Meeting (IEEE APS/URSI). His research interests include analysis and the design of the IoT/5G antennas for new generation devices.

MARTA CABEDO-FABRÉS (Member, IEEE) was born in Valencia, Spain, in 1976. She received the M.S. and Ph.D. degrees in telecommunication engineering from the Universitat Politècnica de València (UPV), Spain, in 2001 and 2007, respectively. In 2001, she joined the Electromagnetic Radiation Group, UPV, as a Research Assistant. In 2004, she became an Associate Professor with the Communications Department, UPV. She has also been the Vice-Director of quality and accreditation at the Telecommunication Engineering Faculty, since 2015. Her current research interests include numerical methods for solving electromagnetic problems, and design and optimization techniques for wideband and multi-band antennas.

EVA ANTONINO-DAVIU (Member, IEEE) was born in Valencia, Spain, in 1978. She received the M.S. and Ph.D. degrees in electrical engineering from the Universitat Politècnica de València, Valencia, in 2002 and 2008, respectively. In 2005, she joined the Communications Department, Universitat Politècnica de València, as an Assistant Professor, where she became an Associate Professor, in 2012. In 2005, she joined the Institute of Telecommunications and Multimedia Applications (iTEAM), where she became the Vice-Director of research, in 2016. In 2005, she stayed as a Guest Researcher at the Department of Antennas & EM Modelling, IMST, Kamp-Lintfort, Germany; at the Laboratory of Electronics, Antennas and Telecommunications (LEAT), University of Nice Sophia-Antipolis, France, in 2018; and at the ATHENA Group, Georgia Institute of Technology, Atlanta, GA, USA, in 2019. She has published more than 200 papers in renowned journals and conferences in the field of antennas and propagation, as well as two book chapters. Her current research interests include characteristic modes, small antennas, wideband and multi-band antenna design, and antenna design for MIMO, the IoT, and mm-wave applications. She was a recipient of the 2019 IEEE AP-S Lot Shafai Mid-Career Distinguished Achievement Award, for her contribution to the systematic design of antenna systems for practical applications using characteristic modes and promoting access of women to engineering. She is an Associate Editor of *IEEE Antennas and Propagation Magazine*. Since 2018, she has been leading the EurAAP Working Group on small antennas.

MIGUEL FERRANDO-BATALLER (Life Member, IEEE) was born in Alcoy, Spain, in 1954. He received the M.Sc. (Ing.) and Ph.D. (Doctor Eng.) degrees in electrical engineering (telecommunication engineering) from the Technical University of Catalonia (UPC), Barcelona, Spain, in 1977 and 1982, respectively.

He has been Research Assistant with the Antennas, Microwave, and Radar Group, Communications Department, Telecommunication Engineering School, UPC, in 1977, where he was an Associate Professor, in 1982. In 1990, he joined the Universitat Politècnica de València (UPV), Valencia, Spain, where he is currently a Full Professor and a Leader of the Antenna and Propagation Laboratory. From 1991 to 1996, he was the Director of the Telecommunication Engineering School, UPV. From 1996 to 1999 and from 2005 to 2009, he was the UPV Vice-Rector for academic planning and information and communication technologies. From 2009 to 2013, he was the Director of the Lifelong Learning Center, UPV. He has authored more than 200 technical articles, conference publications, and book chapters in specialized volumes. His current research interests include antennas, electromagnetic scattering, numerical methods, antenna design, and e-learning activities.

• • •